

# Relaxed hover solutions for multicopters: application to algorithmic redundancy and novel vehicles

**Mark W. Mueller\*** and **Raffaello D'Andrea**

*Institute for Dynamic Systems and Control, ETH Zurich, Switzerland*

## Abstract

*This paper presents a relaxed definition of hover for multicopters with propellers pointing in a common direction. These solutions are found by requiring that the multicopter remain substantially in one position, and that the solutions be constant when expressed in a coordinate system attached to the vehicle. The vehicle's angular velocity is then shown to be either zero or parallel to gravity. The controllability of a vehicle's attitude about these solutions is then investigated. These relaxed hover solutions may be applied as an algorithmic failsafe, allowing for example a quadcopter to fly despite the complete loss of one, two, or three of its propellers. Experimental results validate the quadcopter failsafe for two types of failure (a single propeller, and two opposing propellers failing), and a nonlinear simulation validates the remaining two types of failure (two adjacent, and three propellers failing). The relaxed hover solutions are also shown to allow a multicopter to maintain flight in spite of extreme centre of mass offsets. Finally, the design and experimental validation of three novel vehicles is presented.*

## 1. Introduction

Multicopters have found broad use as research platforms, used e.g. for vision based pose estimation with quadcopters (Fraundorfer et al. 2012) and hexacopters (Weiss et al. 2013), and also as platforms allowing for new capabilities. For example, the use of both quadcopters and hexacopters for whale monitoring is investigated by Selby et al. (2011), and hexacopters are used by Rasmussen et al. (2013) for weed research; a team of quadcopters is used to carry a slung load by Fink et al. (2011) and an octocopter is used to calibrate radio telescope antennae by Hörandel et al. (2013). Multicopters also hold promise as goods delivery vehicles (D'Andrea 2014).

These vehicles typically consist of an even number of propellers all pointing in a common direction, with half of the propellers having the opposite handedness from the remainder, and thus also rotating in the opposite direction. The propellers are then mechanically arranged such that the torques they produce can be made to sum to zero while the propeller thrusts support the vehicle's weight. Differences between propeller thrusts allow the vehicle's attitude to be changed, and the sum of the thrusts is used to accelerate the vehicle. This paper will only consider multicopters where all propellers have

---

\* Corresponding author, email:mwm@ethz.ch

parallel axes of rotation (note however, that alternative designs exist where this is not the case, e.g. Voyles & Jiang (2012) or Efraim et al. (2015)).

Amongst others, a motivation for using a multicopter with six or more propellers, instead of a four propeller quadrocopter, is that the vehicle is able to maintain normal flight if one of the propellers fails (see e.g. Scaramuzza et al. (2014) for a hexacopter design and Marks et al. (2012) for an octocopter rotor failure strategy). The need for having more than four propellers follows from the requirement that the vehicle be able to hover with zero angular velocity even after the failure of one of the actuators.

In this paper, this requirement of having zero angular velocity is relaxed, and instead hover solutions are searched for during which the position remains approximately constant, and where the solutions may be described with constant parameters: these relaxed hover solutions form a superset of those typically used for multicopters. This means that the vehicle may rotate at a constant velocity in hover. They allow for the design of novel hover-capable vehicles, and may also be employed to offer redundancy for multicopters experiencing an actuator failure. Since the solutions are constant in the body frame the powerful techniques of linear time invariant systems theory may be applied for analysis and control design.

An approach is presented to formulate and solve for such relaxed hover solutions, and for designing linear, time invariant controllers to control a hovering vehicle. This approach is used to compute solutions for a quadrocopter experiencing any combination of up to three complete propeller failures. For two of the cases, experimental validation is provided, while the approach for the remaining two types of failure are validated in a nonlinear simulation. The case of losing two opposing propellers is investigated in detail, with a specific focus on vehicle mass and aerodynamic properties that would render the vehicle uncontrollable.

The approach may also be used to control a multicopter where the centre of mass is located far from the propellers' geometric centre. A specific example is given for a quadrocopter with an eccentric centre of mass, where the conventional hover solution of zero angular velocity requires infeasible motor forces. However, by allowing the vehicle to rotate, a feasible solution is found, even if the centre of mass lies outside of the propellers' convex hull.

The methods presented are also applied to design novel, rotating body vehicles. A family of such vehicles, called "spinners", is presented, where each vehicle comprises a number of propellers arranged in a rotationally symmetric pattern about the vehicle's centre of mass, and all propellers have the same handedness and rotate in the same direction. At hover these vehicles rotate at a high angular velocity, in the opposite direction of their propellers. A two, three, and four propeller spinner is presented. In addition to their dynamic properties, when equipped with a camera, such a vehicle could be used as a low-cost omnidirectional flying camera, similar to e.g. Haus et al. (2013) or Youngren et al. (2009) – note however that the spinners tend to rotate at higher velocity than the vehicles in these references, such that motion blur might present a problem.

### *1.1. Related work*

A survey on fault detection and diagnosis and fault-tolerant control strategies for unmanned rotary wing vehicles is given by Zhang et al. (2013), and examples of commercial solutions are the emergency parachutes of Fruity chutes (2014) or those described by Dronologista (2014). Partial failure of a quadrocopter actuator is investigated for example in Ranjbaran & Khorasani (2010), Izadi et al. (2011) and Chamseddine et al. (2012). Complete propeller failure of a single propeller of a quadrocopter is investigated in Freddi et al. (2011), Akhtar et al. (2013), and Lanzon et al. (2014), where the strategy is to give up controlling the vehicle's yaw angle, and use the remaining propellers to achieve a horizontal spin. A flight strategy to cope with an actuator failure on an octocopter is presented in Marks et al. (2012), and a hexacopter design with a focus on actuator redundancy is presented in Achtelik et al. (2012).

The failsafe method presented in this paper extends those above by finding solutions when using fewer than three propellers. Furthermore, this paper presents a family of solutions when using only three propellers (such as a quadcopter having lost one propeller) – the user may thus select the solution most appropriate to the vehicle and the situation.

The controllability of a flying, rotating vehicle with three mutually orthogonal propellers is analysed in Kataoka et al. (2011), and a circular flight path for this vehicle is designed for it in Kataoka et al. (2013) – the vehicle concept uses forward tilted propellers to induce rotation of the vehicle, so that the vehicle then also spins about an axis similarly to the spinners proposed in this work.

This paper will focus on vehicles that do not rely on aerodynamic effects (apart from drag and the propellers) for their stability – this is in contrast to maple-seed-like vehicles such as the Samara (Ulrich et al. 2010), or vehicles like the Spincopter (Orsag et al. 2013).

This work follows on a conference paper published previously (Mueller & D’Andrea 2014), and extends the results by

- presenting a more detailed derivation of the salient effects acting on a multicopter,
- deriving general conditions of the hover solutions without assumptions on the number of propellers, the locations of the propellers, or the mass distribution of the vehicle,
- likewise deriving a general framework for establishing attitude controllability,
- considering additionally the failure case of a quadcopter losing two adjacent propellers,
- showing how the relaxed hover solutions may be applied to multicopters with large centre of mass offsets, and
- presenting the design of three novel multicopters.

## 1.2. Notation

Boldface symbols like  $\mathbf{g}$  are used throughout this paper to denote vectors in three-dimensional space, while non-boldface symbols like  $m$  will generally be used for scalars, with exceptions made explicit. The coordinate system in which a vector is expressed will be denoted by a superscript, for example  $\mathbf{g}^E$  expresses  $\mathbf{g}$  in coordinate system  $E$ . Where possible, vectors will be left without expressing them in any coordinate system. A subscript will be used to express a relationship or attribute, for example  $\omega_{BE}$  represents the angular velocity of  $B$  with respect to  $E$ . The short-hand notation  $(p, q, r)$  will be used to compactly denote a column vector.

## 1.3. Organisation

This paper is organised as follows: in Section 2 the dynamic model of a generic multicopter is presented. Hover solutions are derived in Section 3 and the controllability of the vehicle about these solutions is investigated in Section 4. The approach is applied as an actuator failsafe for quadcopters in Section 5, and applied to a quadcopter with a large centre of mass offset in Section 6. A novel family of multicopters is presented in Section 7, and the paper concludes in Section 8.

## 2. Multicopter modelling

This section derives the equations of motion for a multicopter, with a special focus on the attitude dynamics. A model for the thrust force, reaction torque, and mechanical power consumption of a propeller is also presented. The equations are used in later sections to solve for hover solutions, and the power consumption of the propellers is used to compare different solutions.

Fig. 1 shows a multicopter with  $N_p = 3$  propellers. The multicopter has a total mass  $m$  (including propellers), and its position relative to some point fixed in an inertial frame is expressed as  $\mathbf{d}$ . The mass moment of inertia of the multicopter excluding the propellers is  $\mathbf{I}_B$ , and the multicopter is rotating at an angular velocity  $\omega_{BE}$  with respect to the inertial frame.

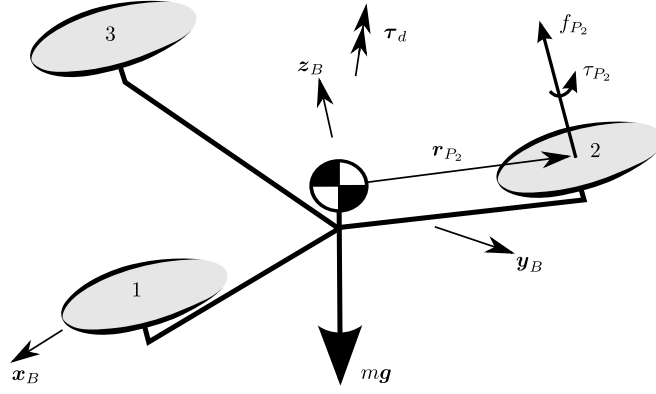


**Fig. 1.** A multicopter with three propellers, showing the definition of the symbols used to derive its dynamics equations. The axes of rotation of the propellers are parallel, and are fixed with respect to the body.

The scalar thrust force  $f_{P_i}$  of each propeller  $i$  points in the body-fixed direction  $\mathbf{z}_B$ , and a body-fixed coordinate system  $B$  is defined so that  $\mathbf{z}_B^B = (0, 0, 1)$ . A perpendicular vector  $\mathbf{x}_B^B = (1, 0, 0)$  is also defined, pointing towards propeller 1. Each thrust force  $i$  acts at a displacement  $\mathbf{r}_{P_i}$  from the multicopter's centre of mass. The angular velocity of propeller  $i$  with respect to the inertial frame is written as  $\boldsymbol{\omega}_{P_i E}$ .

In addition to thrust, each propeller produces a scalar reaction torque  $\tau_{P_i}$  opposing the propeller's angular velocity and parallel to  $\mathbf{z}_B$ , as a result of aerodynamic drag acting on the propeller blade. The mass moment of inertia of propeller  $i$  is  $I_{P_i}$ . As a simplification, because the propellers rotate much faster than the vehicle's body, the propellers will be treated as symmetric about their axes of rotation; their moment of inertia is then constant when expressed in a body-fixed frame, independent of the propeller's instantaneous rotation angle.

It will be assumed that the vehicle travels at low translational velocities, such that translational drag forces may be neglected. For a discussion of such effects see e.g. Martin & Salaün (2010). As a result of the multicopter's angular velocity, a drag torque  $\tau_d$  acts on the multicopter. Gravity acts on the vehicle as a force  $m\mathbf{g}$ .

The translational dynamics of the vehicle, expressed in the inertial coordinate system  $E$ , may now be composed as (Zipfel 2007)

$$m\ddot{\mathbf{d}}^E = \mathbf{z}_B^E \sum_{i=1}^{N_p} f_{P_i} + m\mathbf{g}^E. \quad (1)$$

The orientation of the body with respect to the inertial reference frame is captured by the coordinate transformation matrix  $\mathbf{C}^{EB}$ , such that a vector transforms as  $\mathbf{v}^E = \mathbf{C}^{EB}\mathbf{v}^B$ . The differential equation for this matrix is (Zipfel 2007)

$$\dot{\mathbf{C}}^{EB} = \mathbf{C}^{EB} \llbracket \boldsymbol{\omega}_{BE}^B \rrbracket \quad (2)$$

where  $\llbracket \mathbf{a} \rrbracket$  represents the skew-symmetric matrix form of the cross product, so that  $\llbracket \mathbf{a} \rrbracket \mathbf{b} = \mathbf{a} \times \mathbf{b}$  for any 3D vectors  $\mathbf{a}$  and  $\mathbf{b}$ . Recall that  $\boldsymbol{\omega}_{BE}^B$  represents the vehicle's angular velocity with respect to the inertial frame  $\boldsymbol{\omega}_{BE}$ , as expressed in the body-fixed frame  $B$ . The angular dynamics expressed in the body-fixed coordinate system are (Zipfel 2007)

$$\mathbf{I}_B^B \dot{\boldsymbol{\omega}}_{BE}^B + \sum_{i=1}^{N_p} \mathbf{I}_{P_i}^B \dot{\boldsymbol{\omega}}_{P_i E}^B + \llbracket \boldsymbol{\omega}_{BE}^B \rrbracket \left( \mathbf{I}_B^B \boldsymbol{\omega}_{BE}^B + \sum_{i=1}^{N_p} \mathbf{I}_{P_i}^B \boldsymbol{\omega}_{P_i E}^B \right) = \sum_{i=1}^{N_p} (\llbracket \mathbf{r}_{P_i}^B \rrbracket \mathbf{z}_B^B f_{P_i} + \mathbf{z}_B^B \tau_{P_i}) + \tau_d^B. \quad (3)$$

The first two terms are the time derivative of respectively the vehicle's and the propellers' angular velocities with respect to the inertial frame, as expressed in the body-fixed frame. The third term expresses the cross-coupling of the angular

momentum in the system, due to taking the derivative in a non-inertial frame. The right-hand side of the equation represents all the moments acting upon the body, consisting of the propeller forces acting at a distance from the centre of mass, the propeller reaction torques, and the vehicle drag torque.

### 2.1. Propeller model

It is assumed that the pitch of each of the propellers is fixed and that a given propeller's thrust and torque are functions only of the propeller's angular velocity with respect to the air. Specifically, these functions are taken to be proportional to the square of the angular velocity (Pounds et al. 2002), and the air is assumed to be stationary with respect to the inertial frame. The thrust and torque are then characterised by the propeller coefficients  $\kappa_{f_i}$  and  $\kappa_{\tau_i}$  as follows:

$$f_{P_i} = \kappa_{f_i} (\boldsymbol{\omega}_{P_i E} \cdot \mathbf{z}_B) |\boldsymbol{\omega}_{P_i E} \cdot \mathbf{z}_B| \quad (4)$$

$$\tau_{P_i} = -\kappa_{\tau_i} (\boldsymbol{\omega}_{P_i E} \cdot \mathbf{z}_B) |\boldsymbol{\omega}_{P_i E} \cdot \mathbf{z}_B| \quad (5)$$

with  $\boldsymbol{\omega}_{P_i E} = \boldsymbol{\omega}_{P_i B} + \boldsymbol{\omega}_{B E}$  the rotational velocity of the propeller with respect to the air, and  $\cdot$  denoting the vector inner product. The torque coefficient  $\kappa_{\tau_i}$  is positive, and the sign of  $\kappa_{f_i}$  is a function of the propeller's handedness.

The propeller's scalar speed  $\Omega_{P_i}$  with respect to the body is typically controlled by an electronic speed controller, so that

$$\boldsymbol{\omega}_{P_i B} = \Omega_{P_i} \mathbf{z}_B. \quad (6)$$

Note that this is a very simple propeller model, neglecting for example the translation of the propeller's centre. An example of a more complicated model is given by Martin & Salaün (2010), where a relationship between a quadcopter's translational motion and a horizontal propeller force is given. Such effects are here assumed to be small disturbances, which will be compensated by feedback control.

*Power consumption* The mechanical power consumed by a propeller may be computed as the product of the torque it produces and the angular velocity of the propeller with respect to the body, as given below.

$$P_{P_i} = -\tau_{P_i} \Omega_{P_i}. \quad (7)$$

The mechanical power is used in later sections to compare the efficiency of different hover solutions. This model may be extended, for example, with information about the electrical efficiency of the vehicle's powertrain to compute the power required for the vehicle to hover.

### 2.2. Rotational drag model

The aerodynamic drag torque  $\boldsymbol{\tau}_d$  will in general be very hard to model, and will be a function of the geometry of the vehicle, the angular velocity of the vehicle, and the angular velocities of the propellers. The model used here is based on the form drag of a translating object, where the magnitude of the drag force is quadratic in the magnitude of the translational velocity (McCormick 1995).

Here it is assumed that the magnitude of the torque is quadratic in the vehicle's angular velocity:

$$\boldsymbol{\tau}_d = -\|\boldsymbol{\omega}_{B E}\| \mathbf{K}_d \boldsymbol{\omega}_{B E} \quad (8)$$

where  $\mathbf{K}_d$  is expressed as a constant  $3 \times 3$  matrix in a body-fixed coordinate system, and the Euclidean norm of a vector is written as  $\|\cdot\|$ .

### 3. Hover solutions

The conventional hover condition for a multicopter is at zero acceleration and zero angular velocity, with the thrust vector pointing opposite to gravity. For a symmetric quadcopter in hover, for example, this implies that each motor produces a force equal to one quarter of the vehicle's weight. The propellers' angular momenta then sum to zero, so that the vehicle also has zero total angular momentum in hover. In this situation, the cross coupling in (3) disappears and the vehicle's dynamics in the three translational directions decouple to first order at the equilibrium. An example of a control design for a quadcopter can be found in Mahony et al. (2012).

The definition of hover is relaxed to include flight conditions where the vehicle remains substantially at one point in space, where the vehicle may have non-zero angular velocity. The translational acceleration may likewise be non-zero, but must average to zero for the vehicle to remain substantially in the same position. Only solutions which are constant when described in a body-fixed frame will be considered, with specifically the propellers' angular velocity and the vehicle's angular velocity being constant. These solutions are then time-invariant, allowing for the design of time invariant controllers. The rich literature and powerful tools available for the design and analysis of linear time invariant systems may then be applied. Such a hover solution can be fully described by  $N_p + 6$  variables: the  $N_p$  propeller speeds, three components of the vehicle's angular velocity, and three components of the vehicle's orientation.

#### 3.1. Non-zero angular velocity during hover

If a multicopter's angular velocity with respect to the inertial frame  $\boldsymbol{\omega}_{BE}$  is zero then  $\mathbf{z}_B^E$  is constant, and by (1) the thrust direction  $\mathbf{z}_B$  must point opposite to gravity. The total thrust force must then equal the weight of the vehicle, so that the vehicle has zero acceleration in hover. Furthermore, by (3) the moments produced by the propellers must also sum to zero – this is the conventional hover solution.

For a constant non-zero angular velocity the orientation of the body with respect to an inertial frame at time  $t$  may be solved for in closed form from (2) as

$$\mathbf{C}^{EB}(t) = \mathbf{C}^{EB}(0) \exp(\overline{\|\boldsymbol{\omega}_{BE}^B t\|}) \quad (9)$$

where  $\exp(\cdot)$  is the matrix exponential. An overbar will be used to denote variables that are constant at the hover solution, such as  $\overline{\boldsymbol{\omega}_{BE}^B}$ .

Using Rodrigues' formula (Shuster 1993) and interpreting  $\overline{\boldsymbol{\omega}_{BE}^B} t$  as a rotation vector of constant direction and increasing magnitude, (9) can be solved for explicitly as

$$\exp(\overline{\|\boldsymbol{\omega}_{BE}^B t\|}) = \mathbf{I} + \frac{1}{\overline{\|\boldsymbol{\omega}_{BE}^B\|}} \sin(\overline{\|\boldsymbol{\omega}_{BE}^B\|} t) \overline{\boldsymbol{\omega}_{BE}^B} + \frac{1}{\overline{\|\boldsymbol{\omega}_{BE}^B\|^2}} (1 - \cos(\overline{\|\boldsymbol{\omega}_{BE}^B\|} t)) \overline{\boldsymbol{\omega}_{BE}^B}^2 \quad (10)$$

with  $\mathbf{I}$  the identity matrix. This is periodic, with period  $T_{\text{hvr}} = 2\pi / \overline{\|\boldsymbol{\omega}_{BE}^B\|}$ .

Since all other quantities are constant, the acceleration of the vehicle in hover must also be periodic, with period  $T_{\text{hvr}}$ . The average acceleration of the vehicle can be calculated by averaging (1) over one period, where the time varying quantities have been made explicit below:

$$\frac{1}{T_{\text{hvr}}} \int_0^{T_{\text{hvr}}} m \ddot{\mathbf{d}}^E(t) dt = \frac{1}{T_{\text{hvr}}} \int_0^{T_{\text{hvr}}} \left( \mathbf{z}_B^E(t) \sum_{i=1}^{N_p} \bar{f}_{P_i} + m \mathbf{g}^E \right) dt \quad (11)$$

Transforming  $\mathbf{z}_B^E(t)$  into the body-fixed frame, setting the above equal to zero (so that the average acceleration is zero) and simplifying yields

$$-m\mathbf{g}^E = \frac{1}{T_{\text{hvr}}} \int_0^{T_{\text{hvr}}} \mathbf{C}^{EB}(t) dt \mathbf{z}_B^B \sum_{i=1}^{N_p} \bar{f}_{P_i}. \quad (12)$$

The integral on the right hand side may be thought of as the average coordinate transformation of the vehicle, and can be solved for by substituting (9)-(10):

$$\frac{1}{T_{\text{hvr}}} \int_0^{T_{\text{hvr}}} \mathbf{C}^{EB}(t) dt = \mathbf{C}^{EB}(0) \left( \mathbf{I} + \frac{1}{\|\bar{\boldsymbol{\omega}}_{BE}^B\|^2} \llbracket \bar{\boldsymbol{\omega}}_{BE}^B \rrbracket^2 \right). \quad (13)$$

Substituting and simplifying yields

$$-m\mathbf{g}^E = \left( \frac{\mathbf{z}_B \cdot \bar{\boldsymbol{\omega}}_{BE}}{\|\bar{\boldsymbol{\omega}}_{BE}\|^2} \sum_{i=1}^{N_p} \bar{f}_{P_i} \right) \mathbf{C}^{EB}(0) \bar{\boldsymbol{\omega}}_{BE}^B. \quad (14)$$

A requirement on the total thrust produced can be derived from the above by applying the Euclidean norm:

$$\sum_{i=1}^{N_p} \bar{f}_{P_i} = \frac{m \|\mathbf{g}\| \|\bar{\boldsymbol{\omega}}_{BE}\|}{|\mathbf{z}_B \cdot \bar{\boldsymbol{\omega}}_{BE}|}. \quad (15)$$

Note that this assumes that the sum of the propeller forces is positive.

Substituting (15) into (14) yields the condition that the angular velocity must be parallel to gravity in hover at time 0:

$$\frac{\text{sgn}(\mathbf{z}_B \cdot \bar{\boldsymbol{\omega}}_{BE})}{\|\bar{\boldsymbol{\omega}}_{BE}\|} \mathbf{C}^{EB}(0) \bar{\boldsymbol{\omega}}_{BE}^B = -\frac{1}{\|\mathbf{g}\|} \mathbf{g}^E \quad (16)$$

where  $\text{sgn}(\cdot)$  is the signum function returning the sign of its argument. As it is constant, for any hover solution with constant angular velocity and constant motor forces, the angular velocity always remains parallel to gravity. This also implies that the vehicle's vertical acceleration is always zero in hover.

Given some angular velocity  $\bar{\boldsymbol{\omega}}_{BE}^B$ , the total thrust force produced is constrained by (15), and (16) constrains the vehicle's attitude so that the angular velocity is parallel to gravity. Additionally, the angular acceleration is required to be zero at hover, so that three additional constraints appear from (3):

$$\llbracket \bar{\boldsymbol{\omega}}_{BE}^B \rrbracket \left( \mathbf{I}_B^B \bar{\boldsymbol{\omega}}_{BE}^B + \sum_{i=1}^{N_p} \mathbf{I}_{P_i}^B \bar{\boldsymbol{\omega}}_{P_i}^B \right) = \sum_{i=1}^{N_p} (\llbracket \mathbf{r}_{P_i}^B \rrbracket \mathbf{z}_B^B \bar{f}_{P_i} + \mathbf{z}_B^B \bar{\tau}_{P_i}) + \boldsymbol{\tau}_d^B \quad (17)$$

with  $\bar{f}_{P_i}$  and  $\bar{\tau}_{P_i}$  solved from Section 2.1, and  $\boldsymbol{\tau}_d^B$  from Section 2.2.

There are then seven constraints for the  $N_p + 6$  unknowns, leaving  $N_p - 1$  degrees of freedom for the hover solution. These degrees of freedom may be determined, for example, by finding the hover solution that requires a minimum of input power, by symmetry considerations, or by considerations related to the controllability of the system.

### 3.2. Position trajectory

The vehicle's acceleration in hover will either be constant, or be periodic with period  $T_{\text{hvr}}$ . Specifically, if the vehicle's thrust axis  $\mathbf{z}_B$  is not parallel to the hover angular velocity  $\bar{\boldsymbol{\omega}}_{BE}$ , a component of the total thrust must point perpendicular to

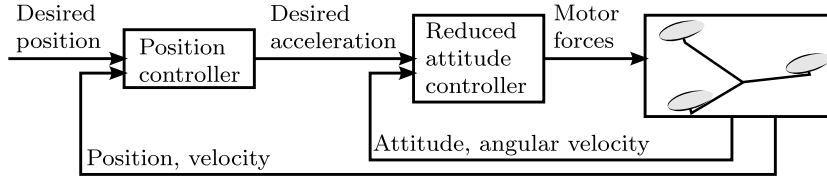


**Fig. 2.** An example cascaded control strategy, where an outer position controller defines a desired acceleration, and an inner controller controls the vehicle's attitude so that the acceleration is achieved.

gravity. Because the vehicle has zero vertical acceleration, the component of the thrust in the direction of the weight must equal the vehicle's weight. The horizontal acceleration component  $\bar{a}_h$  may then be calculated as:

$$(m\bar{a}_h)^2 + (m\|\mathbf{g}\|)^2 = \left( \sum_{i=1}^{N_P} \bar{f}_{P_i} \right)^2. \quad (18)$$

This can be rewritten as a centripetal acceleration of radius  $\bar{r}_{\text{hvr}}$  at vehicle's angular velocity. Substituting the hover forces from (15), and simplifying yields:

$$\bar{r}_{\text{hvr}} = \frac{\|\mathbf{g}\|}{\|\bar{\boldsymbol{\omega}}_{BE}\|^2} \sqrt{\left( \frac{\|\bar{\boldsymbol{\omega}}_{BE}\|}{\mathbf{z}_B \cdot \bar{\boldsymbol{\omega}}_{BE}} \right)^2 - 1}. \quad (19)$$

The vehicle will thus move along a horizontal circle of this radius at the hover solution.

## 4. Position and attitude control

A given hover solution is only useful if the vehicle can enter the solution, and maintain it in the face of disturbances. In this section an approach is given to investigate the controllability of the vehicle about a hover solution. The problem is broken into two sections for ease of analysis: first it is argued that attitude control under constant total thrust is sufficient for position control. An approach is then given for determining the controllability of the attitude system, where the problem is reduced to investigating the controllability of a linear time invariant system with 5 states and  $N_P - 1$  inputs. An example cascaded controller is shown in Fig. 2.

### 4.1. Position control

If both the angular velocity and the total thrust force are constant over one rotation, the average acceleration  $\bar{\mathbf{a}}(t)$  of the vehicle may be defined, similar to what was done in Section 3.1, by averaging  $\ddot{\mathbf{d}}$  over one rotation. The goal is then to control this average acceleration, and thereby the position of the vehicle.

Rather than directly finding an equation for  $\bar{\mathbf{a}}(t)$ , the exposition can be simplified by introducing two unit vectors. A constant body-fixed vector  $\mathbf{n}$  is introduced, which lies parallel to the angular velocity of the vehicle in hover, and is oriented so that it has a positive component in the direction  $\mathbf{z}_B$ . This vector may be thought of as the vehicle's thrust direction, averaged over one period of rotation.

The second unit vector  $\mathbf{n}_{\text{des}}$  is defined through the vehicle's desired acceleration. Introducing the short-hand  $f_{\Sigma}(t)$  for the total thrust force, the vehicle's acceleration averaged over one rotation  $\bar{\mathbf{a}}_{\text{des}}(t)$  may be written as below, from which  $\mathbf{n}_{\text{des}}(t)$  and  $f_{\Sigma}(t)$  may be solved:

$$\bar{\mathbf{a}}_{\text{des}}(t) = \left( \frac{\mathbf{z}_B \cdot \mathbf{n}}{m} f_{\Sigma}(t) \right) \mathbf{n}_{\text{des}}(t) + \mathbf{g}. \quad (20)$$

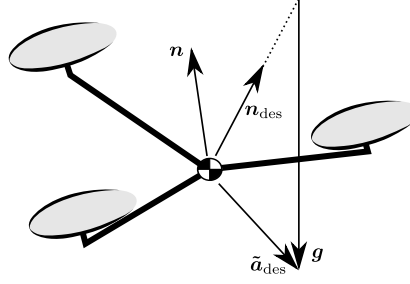


**Fig. 3.** The relationships of the vectors introduced for the position control, where the desired acceleration vector  $\tilde{a}_{des}$  is computed by the position controller, and from this follows the desired normal  $n_{des}$  through (20). The goal of the attitude controller is then to rotate the body-fixed vector  $n$  into  $n_{des}$ .

Note that the factor  $(z_B \cdot n/m)$  is constant. These vectors are visualised in Fig. 3.

Therefore, if the body-fixed vector  $n$  can be controlled to point along some given  $n_{des}$  while the vehicle produces a total thrust force  $f_\Sigma$ , the vehicle's average acceleration will track the desired, and the vehicle's position can be controlled.

#### 4.2. Reduced attitude control

Only the two attitude degrees of freedom relevant to the vehicle's translational motion are controlled, i.e. the unit vector  $n$ . For convenience a control coordinate frame  $C$  is introduced which is fixed with respect to the body-fixed frame  $B$  and where

$$n^C = C^{CB} n^B = (0, 0, 1). \quad (21)$$

The remaining degree of freedom of  $C^{CB}$  (that is, a rotation about  $n$ ) may be chosen arbitrarily. The components  $\alpha_i$  of the angular velocity are introduced, so that

$$\omega_{BE}^C = C^{CB} \omega_{BE}^B = (\alpha_1, \alpha_2, \alpha_3). \quad (22)$$

The time derivative of  $n_{des}^C$  follows from the product rule and (2):

$$\dot{n}_{des}^C = -[\omega_{BE}^C] n_{des}^C + C^{CE} \dot{n}_{des}^E. \quad (23)$$

The change in direction of the desired acceleration vector from (20) is captured by  $\dot{n}_{des}^E$ .

The components  $\eta_i$  are introduced, such that  $n_{des}^C = (\eta_1, \eta_2, \eta_3)$ . The attitude control goal is then to drive  $n_{des}^C$  to  $(0, 0, 1)$ , and drive  $\dot{n}_{des}^C$  to zero. This can be formalised by introducing the state deviation

$$\xi = (\eta_1, \eta_2, \alpha_1, \alpha_2, \alpha_3) - (0, 0, 0, 0, \mathbf{n} \cdot \bar{\omega}_{BE}). \quad (24)$$

If  $\xi$  is stabilisable for some given  $f_\Sigma$ , the vehicle is stabilisable about the desired acceleration.<sup>1</sup>

<sup>1</sup> A stabilisable system is one which can be made asymptotically stable by appropriate state feedback (Callier & Desoer 1994), i.e. any uncontrollable modes are asymptotically stable.

*Selecting input variables* Because the total thrust is fixed at  $f_\Sigma$ , there are  $N_p - 1$  free input variables remaining, which may be used to control the attitude. These may be specified by introducing the input vector  $u$ , and then specifying the motor forces as below:

$$f_{P_i} = \bar{f}_{P_i} + u_i, \text{ for } i \in \{1, \dots, N_p - 1\} \quad (25)$$

$$f_{P_{N_p}} = \bar{f}_{P_{N_p}} - \sum_{i=1}^{N_p-1} u_i. \quad (26)$$

The propeller speeds (instead of thrusts) may alternatively be used as inputs, through the relationships of Section 2.1. The inputs may also be based on symmetry properties of a specific vehicle, so that e.g. independent torques are used as inputs, from which the required propeller speeds are recovered (as is commonly done when controlling quadcopters, e.g. Mahony et al. (2012)).

*Linearised system* The time derivative  $\dot{\xi}$  follows from (3) and (23). For the analysis it will be assumed that  $\dot{\mathbf{n}}_{\text{des}}^E = 0$ , i.e. that the desired average vehicle acceleration in (20) is constant. In practise, a cascaded control strategy as shown in Fig. 2 may be employed, with an outer position controller computing  $\mathbf{n}_{\text{des}}$ . If the dynamics for this outer controller are sufficiently slow, the term  $\dot{\mathbf{n}}_{\text{des}}^E$  in (23) may be neglected.

The effect of the angular acceleration of the propellers with respect to the body,  $\dot{\omega}_{P_i B}^B$ , may be included through a model of the motor dynamics. Alternatively, if the angular inertia of the propellers  $\mathbf{I}_{P_i}^B$  is sufficiently small, this term may be neglected.

Linearising about the hover solution yields a system as below:

$$\dot{\xi} \approx \begin{bmatrix} 0 & \pm \|\bar{\omega}_{BE}\| & 0 & -1 & 0 \\ \mp \|\bar{\omega}_{BE}\| & 0 & 1 & 0 & 0 \\ 0 & 0 & a_{11} & a_{12} & a_{13} \\ 0 & 0 & a_{21} & a_{22} & a_{23} \\ 0 & 0 & a_{31} & a_{32} & a_{33} \end{bmatrix} \xi + Bu \quad (27)$$

where  $a_{ij}$ ,  $B$  and  $u$  depend on the specific vehicle configuration, and follow in part from (3).

The requirement that (27) be stabilisable adds an additional criterion to the search for suitable hover solutions for a vehicle, in addition to the seven algebraic constraints derived in Section 3. Furthermore, (27) may serve as a basis for linear time invariant controller design: in Section 5 controllers are designed for a quadcopter experiencing propeller failures, and in Section 7 controllers are designed for novel vehicles.

## 5. Quadcopter actuator failsafe

Quadcopters are popular as research testbeds, toys, and sensor platforms (e.g. for aerial photography). Compared to hexa- or octocopters, which have six or eight propellers, quadcopters are mechanically simpler and have to carry less structural mass (which in turn may make them more efficient). However, they do not offer an obvious hardware redundancy if a propeller fails (that is, they cannot hover at zero angular velocity after losing a propeller).

In this section it is shown that quadcopters can maintain a hover as defined in Section 3, after the complete loss of a propeller. In fact, under some restrictions on the vehicle's mass distribution and aerodynamic properties, the vehicle remains controllable after the loss of any number of propellers, as long as a single propeller remains operable.

Five different quadcopter failure scenarios are considered:

- no failure,

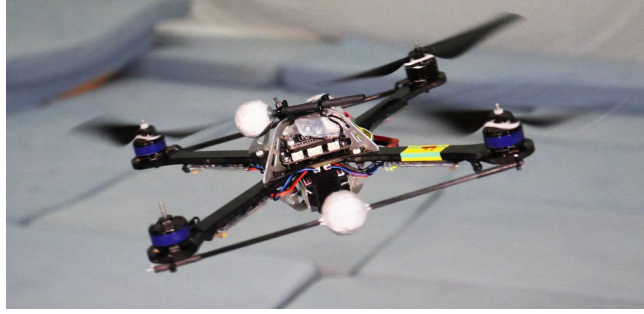


**Fig. 4.** The quadcopter used for the experiments, maintaining controlled flight despite the complete loss of one propeller.

- failure of a single propeller,
- failure of two opposing propellers,
- failure of two adjacent propellers, and
- failure of three propellers.

The hover solutions will first be presented for each, followed by controller design, and then each scenario is validated in a non-linear simulation, For losing a single propeller, and losing two opposing propellers, the simulation is validated by experiment. Extension 1 shows a video of a quadcopter in flight after the loss of a single, and two opposing propellers.

This section focuses on controlled flight near hover in a controlled environment, rather than discussing practical implementation issues related to using these hover solutions on an actual quadcopter in the field. For fault detection strategies, the reader is referred to the references in the introduction. Low-cost and robust sensing/estimation strategies for rapidly rotating vehicles and robust transitions from one flight mode to another may be promising areas of future research.

### 5.1. Platform

The work is validated using quadcopters based on the Ascending Technologies Hummingbird (Gurdan et al. 2007), in the Flying Machine Arena (Lupashin et al. 2014), which will be referred to here simply as “the quadcopter”. Such a quadcopter is shown in Fig. 4.

The vehicle’s mass was measured to be 0.50 kg, and the distance from the centre of mass to the centre of the propellers is 0.17 m. The quadcopter’s inertia was determined from a CAD model, and validated by measuring its period of oscillation when suspended around three different axes. The inertia matrix was estimated to be

$$\mathbf{I}_B^B = \text{diag}(2.7, 2.7, 5.2) \times 10^{-3} \text{kgm}^2. \quad (28)$$

The propeller inertia about its axis of rotation was estimated by approximating the propeller and motor rotor as disks and cylinders, respectively. The remainder of the inertia matrix is neglected, so that the propeller’s inertia is constant when expressed in the body-fixed frame:

$$\mathbf{I}_P^B = \text{diag}(0, 0, 1.5) \times 10^{-5} \text{kgm}^2. \quad (29)$$

The propellers used were characterised using a force-torque sensor, and the thrust and reaction torque coefficients were estimated as  $|\kappa_{f_i}| = 6.41 \times 10^{-6} \text{Ns}^2 \text{rad}^{-2}$  and  $\kappa_{\tau_i} = 1.1 \times 10^{-7} \text{Nm s}^2 \text{rad}^{-2}$ , respectively. On a static test bench, the propellers are able to produce thrust forces in the range of 0.2 N to 3.8 N.

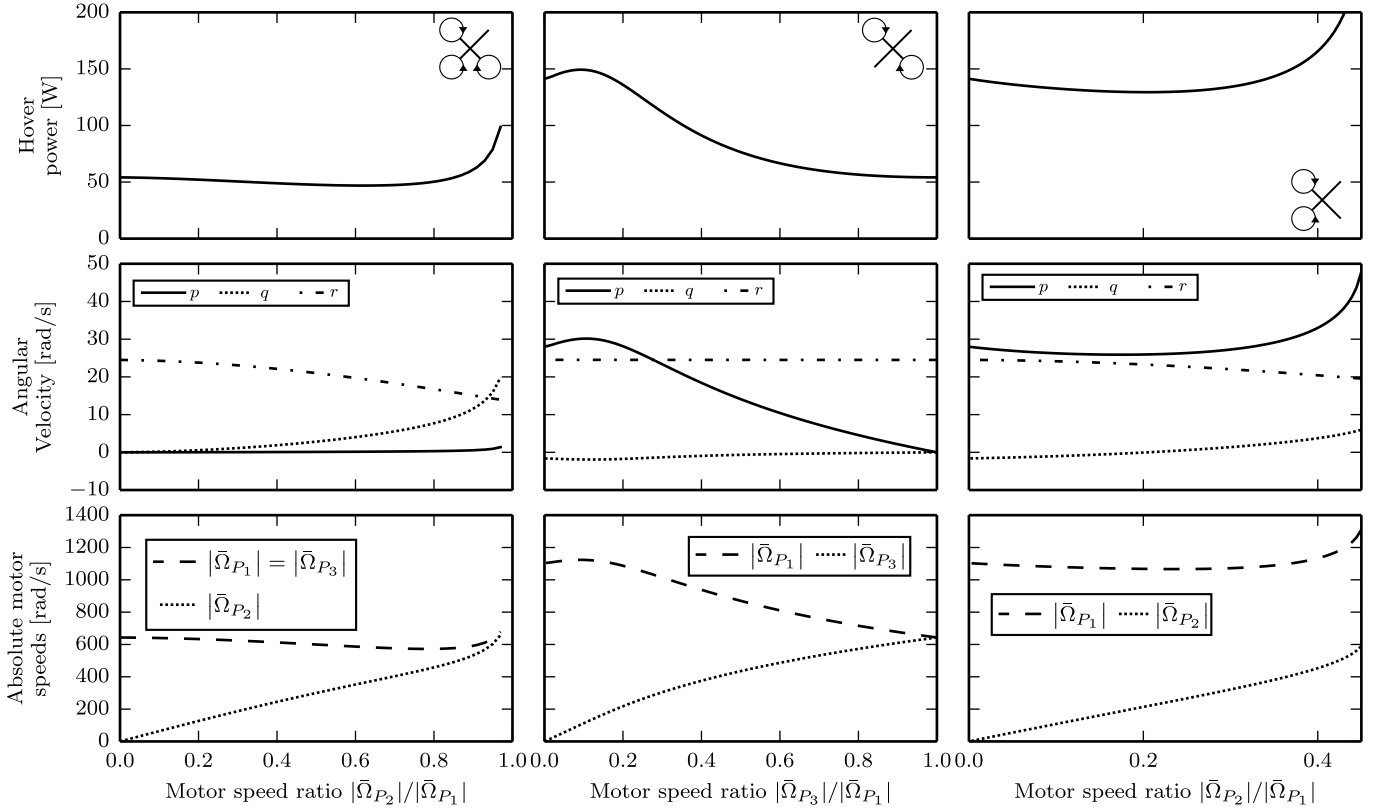


**Fig. 5.** Hover solutions for different failure scenarios, from left to right: failure of a single propeller, failure of two opposing propellers, and failure of two adjacent propellers. The graphs depict how the hover solutions vary as a function of the ratio of angular velocities of the remaining motors. For the single failure, solutions may also be found where the odd propeller turns faster than the two propellers with the same handedness – these are not shown as they consume much more power than the solutions shown. For both scenarios of two propellers failing only half of the possible solutions are shown with the remainder following by symmetry – e.g. for two opposing propellers failing, hover solutions exist with  $\bar{\Omega}_3/\bar{\Omega}_1 > 1$ . The angular velocity is plotted as expressed in the body-fixed coordinate system, where  $\bar{\omega}_{BE}^B = (p, q, r)$ . Note that the propeller speeds shown are absolute.

The aerodynamic drag torque acting on the body was estimated to be diagonal in the body-fixed frame, with entries experimentally identified as below.

$$\mathbf{K}_d^B = \text{diag}(0.7, 0.7, 1.4) \times 10^{-4} \text{Nms}^2 / \text{rad}^2 \quad (30)$$

## 5.2. Hover solutions

Two short-hand notations will be used in this section: the total mechanical power consumed by the propellers will be expressed as  $P_\Sigma = P_{P_1} + P_{P_2} + P_{P_3} + P_{P_4}$ . The propeller speeds  $\Omega_{P_i}$  will be collected into the vector  $\Omega = \{-\Omega_{P_1}, \Omega_{P_2}, -\Omega_{P_3}, \Omega_{P_4}\}$ , where the signs of the entries are changed so that all entries are positive if the propellers spin in their intended directions.

All configurations with more than one remaining functional propeller have at least one degree of freedom in selecting a hover solution. In such cases, numerical optimisation is used to find the hover solution that uses least mechanical power, as computed in Section 2.1. Depending on the application, minimising other variables may be more useful, e.g. minimising the vehicle's total rotation rate, or maximising the minimum distance from the equilibrium propeller speeds to the actuator limits.

*No failure* For the quadcopter with no propellers having failed there are 3 degrees of freedom for finding a hover solution. As expected, the minimum power solution is to have all propellers turning at angular velocities of equal magnitude, and specifically

$$\bar{\Omega} = (438, 438, 438, 438) \text{ rad s}^{-1} \quad (31)$$

$$\bar{\omega}_{BE}^B = (0, 0, 0) \text{ rad s}^{-1} \quad (32)$$

$$\bar{P}_\Sigma = 36.9 \text{ W} \quad (33)$$

$$\bar{r}_{\text{hvr}} = 0 \text{ mm.} \quad (34)$$

*Failure of a single propeller* Without loss of generality it will be assumed that propeller 4 has failed, that is the propeller pointing to the right if looking at the quadcopter from the top. In this case the constraint  $\bar{\Omega}_4 = 0$  is added and two degrees of freedom remain for the hover solution. Through numerical optimisation the following solution was found to consume least power in hover:

$$\bar{\Omega} = (585, 362, 585, 0) \text{ rad s}^{-1} \quad (35)$$

$$\bar{\omega}_{BE}^B = (0.2, 4.3, 19.5) \text{ rad s}^{-1} \quad (36)$$

$$\bar{P}_\Sigma = 46.8 \text{ W} \quad (37)$$

$$\bar{r}_{\text{hvr}} = 6 \text{ mm.} \quad (38)$$

Some intuition for this may be gained by constraining  $\bar{\Omega}_1 = \bar{\Omega}_3$ , and performing a line search over the ratio  $\bar{\Omega}_2/\bar{\Omega}_1$ . This is illustrated in Fig. 5.

*Failure of two opposing propellers* Here it will be assumed that the left and right hand side propellers have failed, so that  $\bar{\Omega}_4 = \bar{\Omega}_2 = 0$ . Now there is only one degree of freedom for the hover solution, which may be explored with a line search over the ratio of the remaining propeller speeds:  $\bar{\Omega}_3/\bar{\Omega}_1$ . This line search is illustrated in Fig. 5. The least power solution is for  $z_B$  to point opposite to gravity, with the two remaining propellers rotating at equal speeds:

$$\bar{\Omega} = (643, 0, 643, 0) \text{ rad s}^{-1} \quad (39)$$

$$\bar{\omega}_{BE}^B = (0, 0, 24.5) \text{ rad s}^{-1} \quad (40)$$

$$\bar{P}_\Sigma = 54.1 \text{ W} \quad (41)$$

$$\bar{r}_{\text{hvr}} = 0 \text{ mm.} \quad (42)$$

*Failure of two adjacent propellers* If both the right hand side and rear propellers have failed, the two added constraints are  $\bar{\Omega}_4 = \bar{\Omega}_3 = 0$ . Again, only one degree of freedom remains in the hover solution, which is also explored with a line search in Fig. 5. In this case, no hover solution exists for the two remaining propellers rotating at equal speed. Thus, it will be assumed that the magnitude of propeller 1's velocity is larger than that of propeller 2. The least power solution is then:

$$\bar{\Omega} = (1067, 218, 0, 0) \text{ rad s}^{-1} \quad (43)$$

$$\bar{\omega}_{BE}^B = (26.0, 0, 23.3) \text{ rad s}^{-1} \quad (44)$$

$$\bar{P}_\Sigma = 129 \text{ W} \quad (45)$$

$$\bar{r}_{\text{hvr}} = 9 \text{ mm.} \quad (46)$$

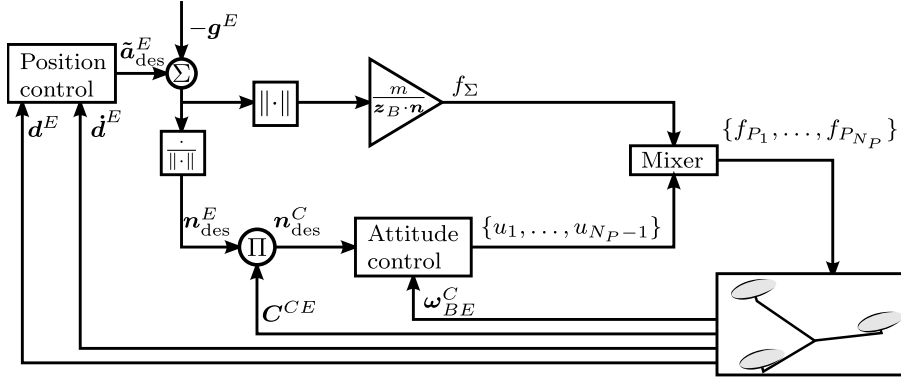


**Fig. 6.** The feedback structure used for the experiments. The position controller computes a desired average acceleration  $\tilde{a}_{des}^E$ , which is then converted into a desired total thrust  $f_\Sigma$  and direction  $n_{des}^E$  according to (20). The attitude controller's outputs  $u_i$  are combined with the desired total thrust force to compute the desired individual propeller forces as in (25)-(26).

Note that a symmetric solution exists for  $|\bar{\Omega}_{P_2}| > |\bar{\Omega}_{P_1}|$ , consuming the same power, but where the vehicle rotates in the opposite direction.

*Failure of three propellers* If all but one propeller have failed, there are no degrees of freedom remaining in the hover solution. It will be assumed that only the front propeller remains, and the hover solution is then

$$\bar{\Omega} = (1103, 0, 0, 0) \text{ rad s}^{-1} \quad (47)$$

$$\bar{\omega}_{BE}^B = (28.0, -1.6, 24.5) \text{ rad s}^{-1} \quad (48)$$

$$\bar{P}_\Sigma = 141 \text{ W} \quad (49)$$

$$\bar{r}_{\text{hvr}} = 8 \text{ mm}. \quad (50)$$

Note that it is unlikely that any practical quadcopter has sufficient excess thrust that a single propeller is able to produce the force required.

### 5.3. Control and validation

The controllability of the vehicle about the hover solution is investigated for each of the five different failure cases presented above. If at least two propellers remain the method of Section 4 was used directly. For the case of losing three propellers (and thus only a single propeller remaining), the method was modified to use the single remaining force as input. In this case, the total force cannot be controlled independently of the attitude. The layout of the controller is shown in Fig. 6, showing the arrangement of the cascaded position and attitude controllers. The controllers are described in more detail below.

*Position control* A position controller was created which calculates a desired acceleration based on the vehicle's current position and velocity, such that the vehicle's position behaves as a damped second order system (Dorf & Bishop 2008). This desired acceleration can then be substituted for the desired average acceleration in (20), and be transformed into a desired vehicle direction  $n_{des}$  and total thrust  $f_\Sigma$ . The second order system's natural frequency and damping ratio were set to  $1.5 \text{ rad s}^{-1}$  and 0.7, respectively.

*Attitude control* Given a linearised attitude system of the form (27), a linear quadratic regulator (LQR) controller (Anderson & Moore 2007) was designed for the attitude system. The same LQR weights are used for each failure scenario. The cost

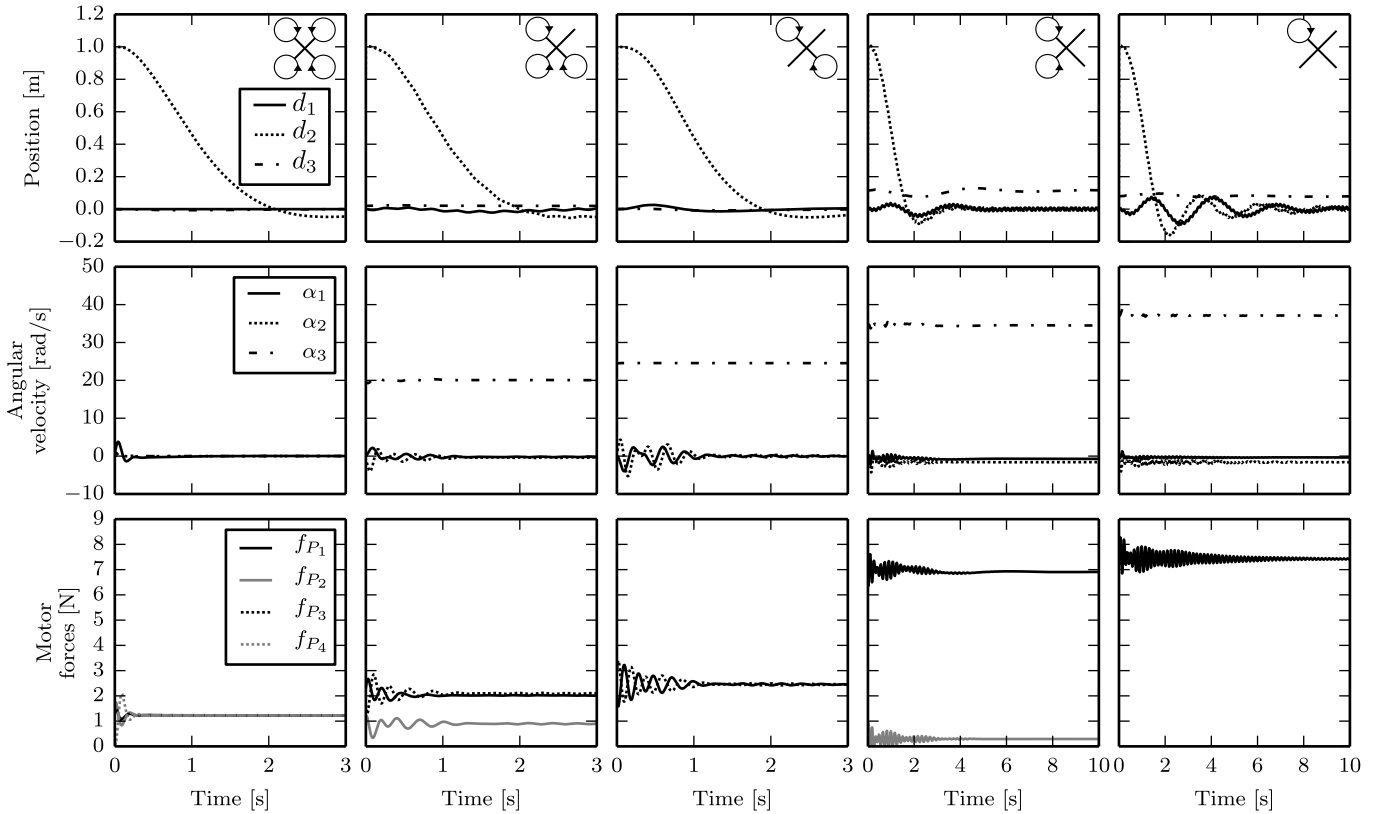


**Fig. 7.** Simulation results for a quadcopter recovering from a 1 m horizontal position error for different failure scenarios. Each column represents a different failure condition, from left to right: no failure (nominal operation), failure of a single propeller, failure of two opposing propellers, failure of two adjacent propellers, failure of three propellers. Note that the angular velocity is expressed in the control frame  $C$ , so that two components must be zero at equilibrium. The position is expressed as  $\mathbf{d}^E = (d_1, d_2, d_3)$ , with  $d_3$  pointing opposite to gravity. The simulation is validated by experiment in Section 5.4. Each row shares its legend. The steady-state vertical offset for the failure of two adjacent propellers and the failure of three propellers is due to a steady state attitude error, as can also be seen in the corresponding steady-state errors of the angular velocity. This error could be explained by interaction between the attitude controller and the position control, and higher-order dynamic effects not compensated for by the linear controller strategy. The steady-state position offsets may be readily compensated for, e.g. by adding an integral term to the position control.

on deviations from the desired normal was set to 20, and the cost on the angular rates set to zero. The input cost was set to the identity matrix of the appropriate size, with units  $N^{-2}$ .

The five dimensional attitude subsystem (27) is stabilisable for each scenario, and is controllable in each case except for two opposing propellers failing. In this case, for the given hover solution, the vehicle's angular velocity about  $z_B$  is uncontrollable. Note that this may be avoided by selecting a different hover condition – this would however increase the hover power consumption and does not actually affect the vehicle's hover performance.

*Simulation results* The control strategy is validated in a nonlinear simulation for each of the different failure scenarios. No sensor noise or external disturbances are simulated. The actuators are simulated to have additional dynamics, so that the propeller speeds respond as a first order system with time constant 15 ms.

A comparison of the flight performance for each failure scenario in simulation is shown in Fig. 7. The data starts with the vehicle at the hover attitude, but with a 1 m horizontal position offset. In each scenario, the vehicle is able to stabilise its position at the origin.

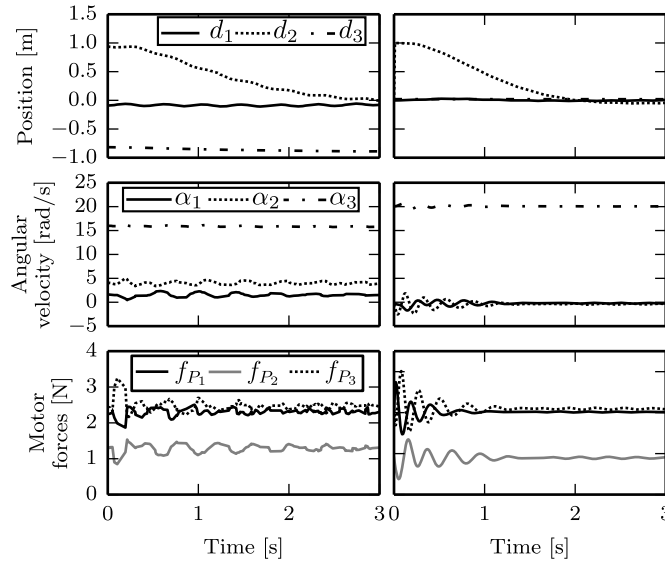


**Fig. 8.** Comparison of experimental (left column) and simulated (right column) data for a quadcopter with a single failed propeller, and an initial 1 m horizontal position error. The angular velocity is as expressed in the control frame  $C$ , and the position is expressed as  $\mathbf{d}^E = (d_1, d_2, d_3)$ . The steady-state vertical position offset of approximately 0.8 m in the experiment is discussed in the text.

#### 5.4. Experimental validation

The simulation is validated by comparing it to data collected from flight experiments in the Flying Machine Arena. The vehicle's state is estimated using position and orientation measurements from a motion capture system, and inertial sensors on the vehicle. A video of such experiments can be found in Extension 1. These experiments are only possible for the scenarios of no failure, failure of a single propeller, and failure of two opposing propellers – for the remaining cases (two adjacent propellers failing or three propellers failing) the quadcopter of Section 5.1 can not produce sufficient thrust to compensate for the vehicle's weight. The data for a single propeller failure are compared in Fig. 8, and for the failure of two opposing propellers in Fig. 9.

For a single failure the experimental data differs somewhat from the simulated data, most notably for the steady-state angular velocity. In experiment, the vehicle has an angular velocity component perpendicular to the  $\mathbf{n}$  axis of approximately  $4.1 \text{ rad s}^{-1}$ . The angular velocity component about  $\mathbf{n}$  is also lower in experiment than expected from the simulation ( $15.8 \text{ rad s}^{-1}$  compared to  $19.9 \text{ rad s}^{-1}$ ). This discrepancy may be due to additional torques acting on the vehicle, specifically torques generated by the translation of the centres of the propellers. Further characterisation of the aerodynamic effects acting on the vehicle at high rotational velocities represent a possibly interesting area of future research.

Furthermore, the vehicle has an approximately 0.8 m vertical offset in experiment for a single failure. This may be partially explained by the angular velocity offset of the experiments w.r.t. the simulation – in the experiment, the quadcopter's thrust axis is tilted farther away from gravity, and thus the feed-forward thrust to compensate for the vehicle's weight from (20) will be too low. This could be readily compensated by e.g. adding an integral control term to the position controller, or by refining the model to allow for better prediction of the vehicle's angular velocity equilibrium. Nonetheless, the controller successfully stabilises the vehicle about the hover solution, and the vehicle's horizontal error is controlled to zero as expected.

For the case of two failed opposing propellers, the simulation matches the experimental data well. It is notable that the two motors do not produce equal force in experiment after the transients have died away – this may be explained by a centre of mass offset of the experimental vehicle, or an imperfection in one of the two actuators.

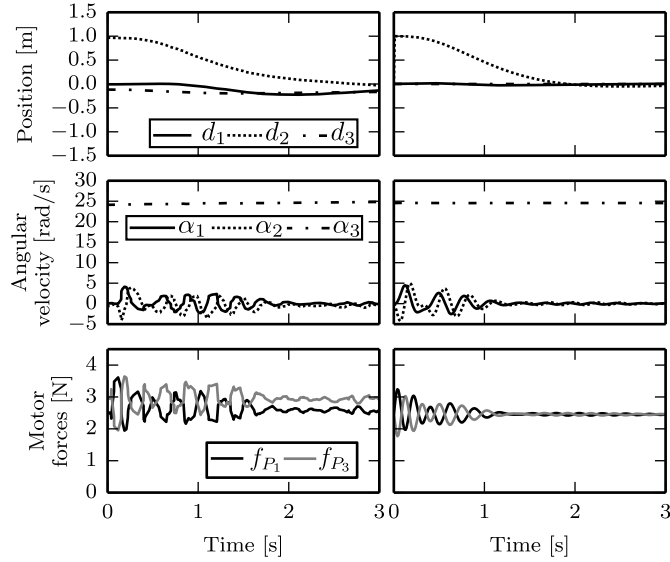


**Fig. 9.** Comparison of experimental (left column) and simulated (right column) data for a quadcopter with two opposing failed propellers, and an initial 1 m horizontal position error. The angular velocity is as expressed in the control frame  $C$ , and the position is expressed as  $\mathbf{d}^E = (d_1, d_2, d_3)$ .

### 5.5. Special cases for controllability

Some intuition for when it is possible to control a quadcopter having lost one or more propellers may be gained by analysing the hover conditions and controllability requirements of Sections 3 and 4 under some simplifying assumptions, especially for the case of losing two opposing propellers.

Specifically, it will be assumed that the vehicle's mass moment of inertia expressed in the body frame is diagonal, with only two unique entries. The inertia of the propeller is assumed to be zero except about its axis of rotation:

$$\mathbf{I}_B^B = \text{diag}(I_{B,xx}, I_{B,xx}, I_{B,zz}) \quad (51)$$

$$\mathbf{I}_P^B = \text{diag}(0, 0, I_{P,zz}) \quad (52)$$

where furthermore  $I_{P,zz} \ll I_{B,zz}$ . The propellers are assumed identical except for their handedness, so that

$$\kappa_{f_i} = (-1)^i \kappa_{f_f} \quad (53)$$

$$\kappa_{\tau_i} = \kappa_{\tau_f}. \quad (54)$$

It is assumed that the vehicle's angular velocity with respect to the inertial frame is much smaller than the propellers' angular velocity with respect to the body, i.e.  $\|\boldsymbol{\omega}_{BE}\| \ll \|\boldsymbol{\omega}_{P_iB}\|$  for each remaining propeller  $i$ . The propellers are mounted at a distance  $l$  from the vehicle's centre of mass.

The vehicle's drag torque coefficient is given below, again with only two unique entries:

$$\mathbf{K}_d^B = \text{diag}(K_{d,xx}, K_{d,xx}, K_{d,zz}). \quad (55)$$

Defining the components of the vehicle angular velocity as  $\boldsymbol{\omega}_{BE}^B = (p, q, r)$ , and applying the simplifications, it follows that:

$$\begin{aligned} \dot{p}I_{B,xx} &= (I_{B,xx} - I_{B,zz})qr - K_{d,xx}p\|\boldsymbol{\omega}_{BE}\| + \\ &\quad l\kappa_f(\Omega_2^2 - \Omega_4^2) - qI_{P,zz}(\Omega_1 + \Omega_2 + \Omega_3 + \Omega_4) \end{aligned} \quad (56)$$

$$\begin{aligned} \dot{q}I_{B,xx} &= (-I_{B,xx} + I_{B,zz})pr - K_{d,xx}q\|\boldsymbol{\omega}_{BE}\| + \\ &\quad l\kappa_f(\Omega_1^2 - \Omega_3^2) + pI_{P,zz}(\Omega_1 + \Omega_2 + \Omega_3 + \Omega_4) \end{aligned} \quad (57)$$

$$\begin{aligned} \dot{r}I_{B,zz} &= -K_{d,zz}r\|\boldsymbol{\omega}_{BE}\| - \\ &\quad \kappa_\tau(|\Omega_1|\Omega_1 + |\Omega_2|\Omega_2 + |\Omega_3|\Omega_3 + |\Omega_4|\Omega_4). \end{aligned} \quad (58)$$

Considering specifically the loss of two opposing motors, such that  $\Omega_2 = \Omega_4 = 0$ , and constraining the hover solution so that  $\bar{\Omega}_1 = \bar{\Omega}_3$ , the hover solution follows as

$$\bar{p} = \bar{q} = 0 \quad (59)$$

$$\bar{r} = \sqrt{\frac{\kappa_\tau m \|\mathbf{g}\|}{\kappa_f K_{d,zz}}} \quad (60)$$

$$\bar{\Omega}_1 = \bar{\Omega}_3 = -\sqrt{\frac{m \|\mathbf{g}\|}{2\kappa_f}}. \quad (61)$$

The attitude controllability can now be analysed as described in Section 4, by introducing the scalar attitude input  $u$  and requiring that the total force remain constant; it follows that  $u = (f_{P_1} - f_{P_3})/2$ . The control frame  $C$  is selected to coincide with the body frame  $B$ . The entries  $a_{ij}$  of the linearised dynamics matrix (27) and the input matrix  $B$  are then as follows:

$$a_{11} = a_{22} = -\frac{K_{d,xx}\bar{r}}{I_{B,xx}} \quad (62)$$

$$a_{33} = -\frac{2K_{d,zz}\bar{r}}{I_{B,zz}} \quad (63)$$

$$a_{12} = -a_{21} = \frac{\sqrt{2m\|\mathbf{g}\|}I_{P,zz}}{\sqrt{\kappa_f}I_{B,xx}} + \frac{(I_{B,xx} - I_{B,zz})\bar{r}}{I_{B,xx}} \quad (64)$$

$$a_{13} = a_{23} = a_{31} = a_{32} = 0 \quad (65)$$

$$B = \frac{2l}{I_{B,xx}} \begin{bmatrix} 0 & 0 & 0 & 1 & 0 \end{bmatrix}^T. \quad (66)$$

It is clear that  $r$  is an exponentially stable, uncontrollable mode of the linearised attitude system, and it will be neglected for the remainder of the analysis. A reduced, four state system remains with a single input. The controllability of this system may be determined by computing the determinant of the  $4 \times 4$  controllability matrix of the system and ensuring that this is non-zero (Callier & Desoer 1994).

After some tedious algebra it emerges that there are two plausible conditions where this system is uncontrollable. Firstly, if (67) holds, the cross-coupling in the attitude dynamics (3) disappears and the vehicle's roll rate  $p$  is uncontrollable:

$$I_{P,zz}\sqrt{2K_{d,zz}} = (I_{B,zz} - I_{B,xx})\sqrt{\kappa_\tau}. \quad (67)$$

If, instead, the following two conditions hold, the system is also uncontrollable:

$$K_{d,xx} = 0 \quad \text{and} \quad (68)$$

$$I_{P,zz} \sqrt{2K_{d,zz}} = (I_{B,zz} - 2I_{B,xx}) \sqrt{\kappa_\tau}. \quad (69)$$

In this case there are two uncontrollable modes, which correspond to  $p + a_{12}\eta_1$  and  $\eta_2$ .

These two conditions may be used to determine whether a quadcopter's attitude will be close to uncontrollable with two opposing propellers, given its physical parameters. Unfortunately, the aerodynamic drag parameters  $K_{d,xx}$  and  $K_{d,zz}$  may be hard to accurately predict.

If only a single propeller has failed, the same hover solution may be selected as when two opposing propellers have failed with  $\bar{p} = \bar{q} = 0$ . Then the system has an additional input which directly actuates the roll rate  $p$ , and it will be controllable for all mass distributions.

*Further simplifications* The preceding results may be given a more intuitive geometric interpretation by further assuming that the propellers have zero inertia, i.e.  $I_{P,zz} = 0$ . The first case for being uncontrollable then simplifies from (67) to the requirement that  $I_{B,xx} = I_{B,zz}$  (recall that by assumption also  $I_{B,xx} = I_{B,yy}$ ). This happens if the vehicle's mass distribution is symmetric, i.e. similar to that of a sphere. The second case for being uncontrollable simplifies from (69) to  $I_{B,zz} = 2I_{B,xx} = 2I_{B,yy}$  – this corresponds to the mass distribution of a two-dimensional object, e.g. a flat plate with the propellers' thrust axes pointing along the plate's normal.

## 6. Quadcopter centre of mass offsets

If a quadcopter's centre of mass is not located at its geometric centre the propeller forces will no longer all be equal when the vehicle hovers at zero angular velocity. Specifically, for the input torques of (3) to balance, propellers closer to the centre of mass must produce larger forces.

For large centre of mass offsets the required propeller forces may be close to (or even exceed) the propeller limits, leaving little or no control authority for feedback control. In such a situation, the approach of Sections 3-4 may be used to find a hover solution where the nominal motor forces are further away from the actuator limits.

As an extreme example: for a quadcopter with propellers distributed on the corners of a square, if the centre of mass is located halfway between the geometric centre of the propellers and one propeller, the propeller farthest from the centre of mass must produce zero force for the input torques to balance. If the centre of mass moves further away from the geometric centre, the far propeller must produce a negative thrust. In this situation, the vehicle will consume significantly more power than if the centre of mass coincides with the geometric centre. Furthermore, specific hardware may not be able to produce negative thrust.

If however the vehicle is allowed to rotate during hover, one may search e.g. for a hover solution that minimizes the required mechanical power, or maximizes the distance from the propellers' thrust in hover to the actuator saturation limits.

As an example, consider the quadcopter of Section 5 carrying an additional load of 0.1 kg at some distance  $\rho$  from the geometric centre of the propellers. As the mass is shifted farther from the vehicle's geometric centre, the vehicle's centre of mass also moves farther from the geometric centre. The ratio of vehicle mass to the additional mass implies that the centre of mass is located at a distance  $\rho/6$  from the geometric centre.

The mass moment of inertia of the vehicle with the added mass may be computed using Huygen's theorem (Zipfel 2007). For the simplicity of analysis, it is assumed that the vehicle's drag matrix  $\mathbf{K}_d$  remains unchanged with the added mass and the resulting shifted centre of mass.

Fig. 10 compares the motor speeds and power requirements of the quadcopter as the mass is moved farther away from the geometric centre, for both the conventional hover solution (with zero angular velocity) and the relaxed hover solution of

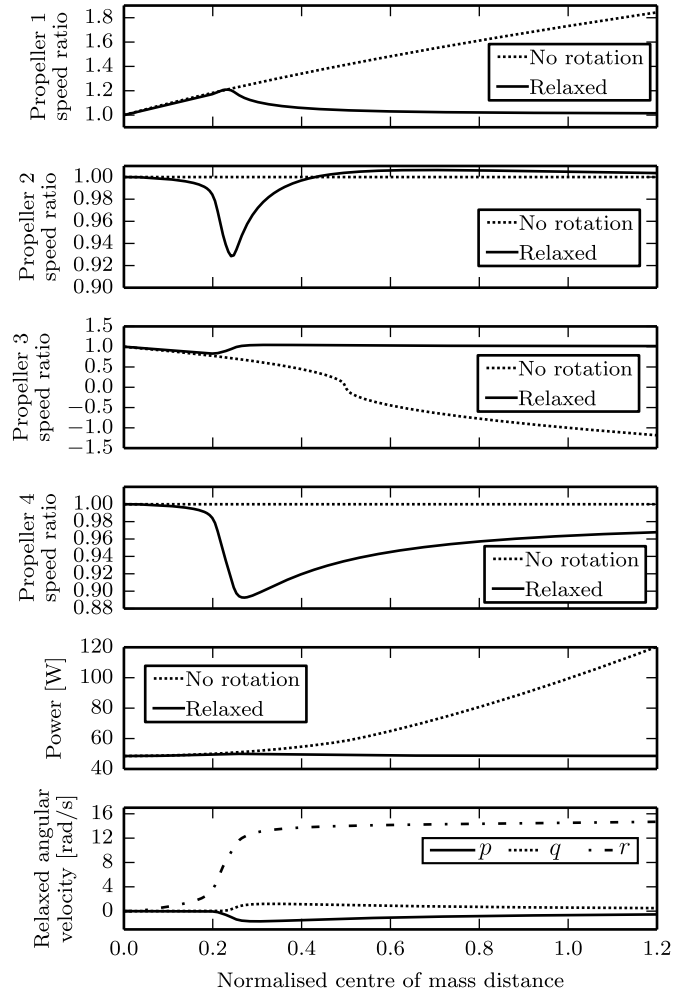


**Fig. 10.** Hover solutions for a quadcopter with an additional mass mounted at varying distances from the vehicle's geometric centre, showing the solution at which the vehicle has zero angular velocity, and a relaxed hover solution of Section 3 that minimizes power consumption. Note that the abscissa is the distance of the centre of mass to the geometric centre, normalised by the quadcopter's arm length. Because of the mass ratio, the additional mass is placed six times farther from the propellers' geometric centre than the resulting centre of mass. The top four graphs plot for each propeller the ratio of each required propeller speed to that speed required if the centre of mass coincides with the geometric centre. The bottom graph shows the three components of the vehicle's angular velocity in the relaxed hover solution expressed in the body-fixed frame, where  $\omega_{BE}^B = (p, q, r)$ .



**Fig. 11.** A novel class of flying vehicles, from left to right: bispinner, trispinner, and quadspinner. For each vehicle, all propellers rotate in the same direction, causing the vehicle to rotate in the opposite direction in hover. Extension 2 contains a video showing each of these vehicles flying.

Section 3. The mass is moved from the geometric center along the axis pointing towards propeller 1. For the conventional hover solution, the power required increases significantly as the mass is moved outwards, and at distances of  $\rho > 0.51$  m the propeller farthest from the added mass must rotate in the direction opposite to the usual.

The figure also shows the results if the vehicle is allowed to rotate, and a search is done to find motor speeds that minimise the mechanical power in hover. The vehicle’s mechanical power remains within 5% of the nominal power, even with displacements up to  $\rho = 1.2$  m. The motor speeds also remain close to the nominal speeds, even at large displacements. Note that for  $\rho > 1.02$  m the centre of mass lies outside of the convex hull of the four propellers.

Thus, if the propeller’s direction of rotation is fixed, a quadcopter may be operated under a much wider range of centre of mass positions with the relaxed hover conditions compared to the restriction that the vehicle’s angular velocity is zero at hover.

## 7. Novel vehicles

A novel class of hover-capable vehicles may also be designed using the approach of Section 3. Here, three examples are given, with novel vehicles having two, three, or four propellers arranged symmetrically about the vehicle’s centre of mass. The propellers are mounted such that their thrust axes are parallel, and all propellers have the same handedness.

This family of vehicles is dubbed “spinners”, allowing a prefix for the number of propellers. A quadspinner, trispinner, and bispinner are shown in Fig. 11, and Extension 2 contains a video showing each vehicle in flight. Because of their symmetries, the hover equilibria are chosen such that all propellers have the same rotational speed.

Each vehicle is controlled similarly to the quadcopter in Fig. 6, where the position and attitude control are separated. A desired attitude is generated by the position controller, which makes the position behave like a second order damped system. An LQR controller is created for the attitude, based on the first order model of Section 4.

The notation of Section 5.2 will be used to describe the hover solutions, and again so that all entries in  $\bar{\Omega}$  are nominally positive:  $\bar{\Omega} = \{-\Omega_{P_1}, \dots, -\Omega_{P_{N_p}}\}$ . The motors and propellers used are the same as those of Section 5.1.

### 7.1. Quadspinner

A normal quadcopter may easily be converted into a quadspinner, by reversing the direction of rotation of two motors (and accordingly replacing the propellers). The quadspinner shown in Fig. 11 has the same physical properties as the quadcopter presented in Section 5.1, except for the propellers’ handedness.

It will then hover at the following condition:

$$\bar{\Omega} = (462, 462, 462) \text{ rad s}^{-1} \quad (70)$$

$$\bar{\omega}_{BE}^B = (0, 0, 24.2) \text{ rad s}^{-1} \quad (71)$$

$$\bar{P}_{\Sigma} = 38.9 \text{ W}. \quad (72)$$

## 7.2. Trispinner

A three propeller vehicle was also created, with the propellers mounted at intervals of  $120^\circ$ . Conceptually, this trispinner is very similar to the quadspinner, as the propellers can produce a torque in any direction in the plane perpendicular to the thrust vector, for some given total thrust value.

Visually similar tri-rotor vehicles exist (see for example Salazar-Cruz et al. (2006), Zou et al. (2012)) that use a servo motor in addition to the three propellers, where the servo motor can rotate one of the vehicle's arms and thus vector the thrust of one propeller. These vehicles can then fully control their attitudes in addition to their total thrust. The trispinner, in comparison, does not attempt to control its orientation about the thrust axis, and has the advantage of being mechanically simpler.

The vehicle depicted in Fig. 11 has a mass of 0.44 kg, with the propellers mounted 0.17 m from the vehicle's centre of mass. The vehicle's inertia matrix and drag characteristics are then given below:

$$\mathbf{I}_B^B = \text{diag} (2.4, 2.3, 4.4) \times 10^{-3} \text{ kg m}^2 \quad (73)$$

$$\mathbf{K}_d^B = \text{diag} (0.55, 0.55, 1.1) \times 10^{-4} \text{ Nms}^2 / \text{rad}^2 \quad (74)$$

and the hover condition is then

$$\bar{\Omega} = (498, 498, 498) \text{ rad s}^{-1} \quad (75)$$

$$\bar{\omega}_{BE}^B = (0, 0, 26.1) \text{ rad s}^{-1} \quad (76)$$

$$\bar{P}_{\Sigma} = 36.6 \text{ W}. \quad (77)$$

## 7.3. Bispinner

Finally, a bispinner was created, by removing two complete arms from a quadcopter. The vehicle has a mass of 0.38 kg, and the inertia matrix and drag characteristics are as below:

$$\mathbf{I}_B^B = \begin{bmatrix} 270 & 65 & 0 \\ 65 & 3300 & 0 \\ 0 & 0 & 3400 \end{bmatrix} \times 10^{-6} \text{ kg m}^2 \quad (78)$$

$$\mathbf{K}_d^B = \text{diag} (0, 3.6, 7.2) \times 10^{-5} \text{ Nms}^2 / \text{rad}^2. \quad (79)$$

Note that the vehicle's inertia about the axis connecting the motors is an order of magnitude smaller than the other terms on the diagonal. The off-diagonal terms follow as a result of the battery being positioned at an angle.

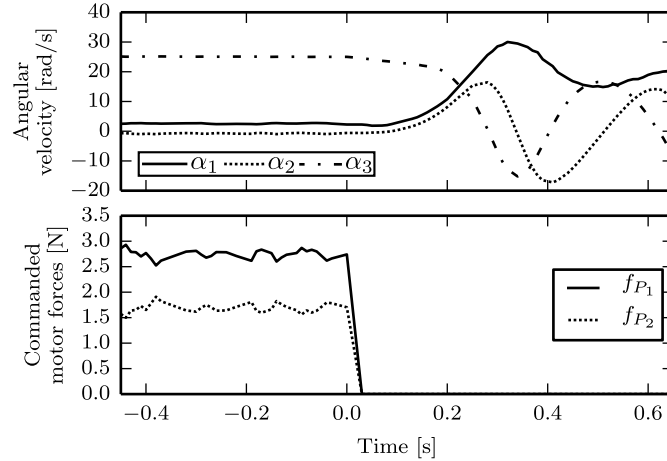


**Fig. 12.** Experimental data for a bispinner at hover, where the motors (and thus attitude control) are switched off at time 0. The open loop exponential instability of the angular velocity is clearly visible, and angular accelerations up to  $450 \text{ rad s}^{-2}$  are measured by the vehicle's rate gyroscopes.

The hover condition for this vehicle is

$$\bar{\Omega} = (567, 567) \text{ rad s}^{-1} \quad (80)$$

$$\bar{\omega}_{BE}^B = (0, -0.1, 29.7) \text{ rad s}^{-1} \quad (81)$$

$$\bar{P}_{\Sigma} = 36.1 \text{ W}. \quad (82)$$

Because of its mass distribution, this vehicle has some unique dynamic properties compared to the tri- and quadspinner. The matrices of the linearised attitude system, computed with the method of Section 4, are as below:

$$A = \begin{bmatrix} 0 & 29.7 & 0 & -1 & 0 \\ -29.7 & 0 & 1 & 0 & 0 \\ 0 & 0 & 1.6 & 54.1 & -0.2 \\ 0 & 0 & 22.8 & -2.0 & 0 \\ 0 & 0 & 0 & 0 & -1.3 \end{bmatrix} \quad (83)$$

$$B = \begin{bmatrix} 0 & 0 & 24.9 & -103.5 & 0.3 \end{bmatrix}^T. \quad (84)$$

This linearised system has a single exponentially unstable mode, with eigenvalue at 35.2. This open loop instability can be clearly seen in Fig. 12.

## 8. Conclusion and outlook

This paper presents a broadened definition of hover for multicopters, where specifically the vehicle is not constrained to have zero angular velocity when hovering. The class of vehicles that can achieve these hover conditions are a superset of conventional multicopters.

By allowing a conventional multicopter to hover at non-zero angular velocity, it is shown that the vehicle can maintain controlled flight despite the complete loss of all but one propeller. This seems particularly relevant in the case of quadcopters, as this negates one of the main arguments for using hexacopters or octocopters instead of quadcopters. As such, the use of the proposed failsafe solutions may allow for a more widespread use (and greater public acceptance of)

quadcopters. The extended hover solutions are also shown to allow a quadcopter to maintain flight under large centre of mass disturbances.

Novel vehicles may also be conceived, such as the spinners presented herein. These vehicles could be used as novel hobbyist platforms or toys, or could be used as novel sensing platforms. For example, by mounting a line scanner to such a vehicle, and using the vehicle's angular velocity to sweep the sensor over the environment, a mechanically simple omnidirectional sensor can be created from a line scanner.

## Acknowledgements

The Flying Machine Arena is the result of contributions of many people, a full list of which can be found at [http://www.idsc.ethz.ch/Research/\\_DAndrea/FMA/participants](http://www.idsc.ethz.ch/Research/_DAndrea/FMA/participants). The authors would like to thank Alex Wilkinson for his help designing the trispinner.

## Funding

This research was supported by the Swiss National Science Foundation (SNSF), under grant application 138112.

## References

- Achtelik, M. C., Doth, K.-M., Gurdan, D. & Stumpf, J. (2012), Design of a multi rotor MAV with regard to efficiency, dynamics and redundancy, in 'AIAA Guidance, Navigation, and Control Conference', pp. 1–17.
- Akhtar, A., Waslander, S. & Nielsen, C. (2013), Fault tolerant path following for a quadrotor, in 'IEEE Annual Conference on Decision and Control (CDC)', pp. 847–852.
- Anderson, B. D. & Moore, J. B. (2007), *Optimal control: linear quadratic methods*, Courier Dover Publications.
- Callier, F. & Desoer, C. (1994), *Linear System Theory*, Springer Texts in Electrical Engineering, Springer.
- Chamseddine, A., Zhang, Y., Rabbath, C. A., Join, C. & Theilliol, D. (2012), 'Flatness-based trajectory planning/replanning for a quadrotor unmanned aerial vehicle', *IEEE Transactions on Aerospace and Electronic Systems* **48**(4), 2832–2848.
- D'Andrea, R. (2014), 'Can drones deliver?', *IEEE Transactions on Automation Science and Engineering* **11**(3), 647–648.
- Dorf, R. & Bishop, R. (2008), *Modern Control Systems, Eleventh Edition*, Prentice-Hall.
- Dronologista (2014), 'DJI dropsafe system', (Accessed 29 Nov. 2014) <http://robohub.org/dji-dropsafe-system/>.
- Efraim, H., Shapiro, A. & Weiss, G. (2015), 'Quadrotor with a dihedral angle: on the effects of tilting the rotors inwards', *Journal of Intelligent & Robotic Systems* pp. 1–12.
- Fink, J., Michael, N., Kim, S. & Kumar, V. (2011), 'Planning and control for cooperative manipulation and transportation with aerial robots', *International Journal of Robotics Research* **30**(3), 324–334.
- Fraundorfer, F., Heng, L., Honegger, D., Lee, G. H., Meier, L., Tanskanen, P. & Pollefeys, M. (2012), Vision-based autonomous mapping and exploration using a quadrotor MAV, in 'IEEE/RSJ International Conference on Intelligent Robots and Systems (IROS)', IEEE, pp. 4557–4564.
- Freddi, A., Lanzon, A. & Longhi, S. (2011), A feedback linearization approach to fault tolerance in quadrotor vehicles, in 'Proceedings of the 18th IFAC World Congress', pp. 5413–5418.
- Fruity chutes (2014), 'Multicopter, quadcopter, drone, RC aircraft recovery and rescue chutes', (Accessed 29 Nov. 2014) [http://www.fruitychutes.com/uav\\_rpv\\_drone\\_recovery\\_parachutes/multicopter\\_quadcopter-rc-aircraft\\_recovery\\_and\\_rescue\\_chutes.htm](http://www.fruitychutes.com/uav_rpv_drone_recovery_parachutes/multicopter_quadcopter-rc-aircraft_recovery_and_rescue_chutes.htm).
- Gurdan, D., Stumpf, J., Achtelik, M., Doth, K.-M., Hirzinger, G. & Rus, D. (2007), Energy-efficient autonomous four-rotor flying robot controlled at 1 kHz, in 'IEEE International Conference on Robotics and Automation (ICRA)', pp. 361–366.
- Haus, T., Orsag, M. & Bogdan, S. (2013), Omnidirectional vision based surveillance with spincopter, in 'IEEE International Conference on Unmanned Aircraft Systems (ICUAS)', pp. 326–332.

- Hörandel, J. R., Buitink, S., Corstanje, A., Enriquez, J. E. & Falcke, H. (2013), The LOFAR radio telescope as a cosmic ray detector, in 'International Cosmic Ray Conference'.
- Izadi, H. A., Zhang, Y. & Gordon, B. W. (2011), Fault tolerant model predictive control of quad-rotor helicopters with actuator fault estimation, in 'Proceedings of the 18th IFAC World Congress', pp. 6343–6348.
- Kataoka, Y., Sekiguchi, K. & Sampei, M. (2011), Nonlinear control and model analysis of trirotor uav model, in 'Proceedings of the 18th IFAC World Congress', Vol. 18, IFAC, pp. 10391–10396.
- Kataoka, Y., Sekiguchi, K. & Sampei, M. (2013), Circle motion control of trirotor uav via discrete output zeroing, in 'IEEE Annual Conference on Decision and Control (CDC)', IEEE, pp. 226–231.
- Lanzon, A., Freddi, A. & Longhi, S. (2014), 'Flight control of a quadrotor vehicle subsequent to a rotor failure', *Journal of Guidance, Control, and Dynamics* **37**(2), 580–591.
- Lupashin, S., Hehn, M., Mueller, M. W., Schoellig, A. P., Sherback, M. & D'Andrea, R. (2014), 'A platform for aerial robotics research and demonstration: The Flying Machine Arena', *Mechatronics* **24**(1), 41 – 54.
- Mahony, R., Kumar, V. & Corke, P. (2012), 'Aerial vehicles: Modeling, estimation, and control of quadrotor', *IEEE Robotics & Automation Magazine* **19**(3), 20–32.
- Marks, A., Whidborne, J. F. & Yamamoto, I. (2012), Control allocation for fault tolerant control of a VTOL octorotor, in 'UKACC International Conference on Control', IEEE, pp. 357–362.
- Martin, P. & Salaün, E. (2010), The true role of accelerometer feedback in quadrotor control, in 'IEEE International Conference on Robotics and Automation (ICRA)', pp. 1623–1629.
- McCormick, B. W. (1995), *Aerodynamics Aeronautics and Flight Mechanics*, John Wiley & Sons, Inc.
- Mueller, M. W. & D'Andrea, R. (2014), Stability and control of a quadcopter despite the complete loss of one, two, or three propellers, in 'IEEE International Conference on Robotics and Automation (ICRA)'.
- Orsag, M., Cestic, J., Haus, T. & Bogdan, S. (2013), 'Spincopter wing design and flight control', *Journal of Intelligent & Robotic Systems* **70**(1-4), 165–179.
- Pounds, P., Mahony, R., Hynes, P. & Roberts, J. (2002), Design of a four-rotor aerial robot, in 'Australasian Conference on Robotics and Automation', Vol. 27, p. 29.
- Ranjbaran, M. & Khorasani, K. (2010), Fault recovery of an under-actuated quadrotor aerial vehicle, in 'IEEE Annual Conference on Decision and Control (CDC)', IEEE, pp. 4385–4392.
- Rasmussen, J., Nielsen, J., Garcia-Ruiz, F., Christensen, S. & Streibig, J. C. (2013), 'Potential uses of small unmanned aircraft systems (UAS) in weed research', *Weed Research* **53**(4), 242–248.
- Salazar-Cruz, S., Kendoul, F., Lozano, R. & Fantoni, I. (2006), Real-time control of a small-scale helicopter having three rotors, in 'IEEE/RSJ International Conference on Intelligent Robots and Systems (IROS)', IEEE, pp. 2924–2929.
- Scaramuzza, D., Achtelik, M., Doitsidis, L., Friedrich, F., Kosmatopoulos, E., Martinelli, A., Achtelik, M., Chli, M., Chatzichristofis, S., Kneip, L., Gurdan, D., Heng, L., Lee, G. H., Lynen, S., Pollefeys, M., Renzaglia, A., Siegwart, R., Stumpf, J., Tanskanen, P., Troiani, C., Weiss, S. & Meier, L. (2014), 'Vision-controlled micro flying robots: from system design to autonomous navigation and mapping in gps-denied environments', *IEEE Robotics Automation Magazine* **21**(3), 26–40.
- Selby, W., Corke, P. & Rus, D. (2011), Autonomous aerial navigation and tracking of marine animals, in 'Proceedings of the 2011 Australasian Conference on Robotics and Automation', Australian Robotics & Automation Association, pp. 1–7.
- Shuster, M. D. (1993), 'A survey of attitude representations', *The Journal of the Astronautical Sciences* **41**(4), 439–517.
- Ulrich, E. R., Humbert, J. S. & Pines, D. J. (2010), 'Pitch and heave control of robotic samara micro air vehicles', *Journal of Aircraft* **47**(4), 1290–1299.
- Voyles, R. & Jiang, G. (2012), Hexrotor UAV platform enabling dextrous interaction with structures - preliminary work, in 'IEEE International Symposium on Safety, Security, and Rescue Robotics (SSRR)', IEEE, pp. 1–7.
- Weiss, S., Achtelik, M. W., Lynen, S., Achtelik, M. C., Kneip, L., Chli, M. & Siegwart, R. (2013), 'Monocular vision for long-term micro aerial vehicle state estimation: A compendium', *Journal of Field Robotics* **30**(5), 803–831.

- Youngren, H., Jameson, S. & Satterfield, B. (2009), Design of the SAMARAI monowing rotorcraft nano air vehicle, in 'Proceedings of the American Helicopter Society AHS 65th Annual Forum and Technology Display'.
- Zhang, Y., Chamseddine, A., Rabbath, C., Gordon, B., Su, C.-Y., Rakheja, S., Fulford, C., Apkarian, J. & Gosselin, P. (2013), 'Development of advanced FDD and FTC, techniques with application to an unmanned quadrotor helicopter testbed', *Journal of the Franklin Institute* **350**(9), 2396–2422.
- Zipfel, P. H. (2007), *Modeling and Simulation of Aerospace Vehicle Dynamics Second Edition*, American Institute of Aeronautics and Astronautics.
- Zou, J.-T., Su, K.-L. & Tso, H. (2012), 'The modeling and implementation of tri-rotor flying robot', *Artificial Life and Robotics* **17**(1), 86–91.

## **A. Index to multimedia extensions**

The multimedia extensions to this article are at: <http://www.ijrr.org>.

Extension	Media type	Description
1	Video	Quadrocopter failsafe flight experiments
2	Video	Novel vehicles flight experiments